INSTITUTE OF PHYSICS PUBLISHING PLASMA PHYSICS AND CONTROLLED FUSION

Plasma Phys. Control. Fusion **44** (2002) L1–L10 PII: S0741-3335(02)26691-9

LETTER TO THE EDITOR

Two-dimensional simulations of correlation reflectometry in fusion plasmas

E J Valeo, G J Kramer and R Nazikian

Plasma Physics Laboratory, Princeton University, Princeton, NJ 08543, USA

E-mail: valeo@pppl.gov

Received 10 July 2001, in final form 4 December 2001
Published 23 January 2002
Online at stacks.iop.org/PPCF/44/L1

Abstract

A two-dimensional wave propagation code, developed specifically to simulate correlation reflectometry in large-scale fusion plasmas, is described. The code makes use of separate computational methods in the vacuum, underdense and reflection regions of the plasma in order to obtain the high computational efficiency necessary for correlation analysis. Simulations of TFTR plasma with internal transport barriers are presented and compared with one-dimensional full-wave simulations. It is shown that the two-dimensional simulations are remarkably similar to the results of the one-dimensional full-wave analysis for a wide range of turbulent correlation lengths. Implications for the interpretation of correlation reflectometer measurements in fusion plasma are discussed.

1. Introduction

Reflectometry [1,2] is routinely used to infer turbulent fluctuation levels and correlation lengths in both small-scale laboratory plasma [3, 4] and large-scale fusion research devices [5]. The basic technique is to launch an electromagnetic wave with frequency chosen so that there exists a reflection layer in the plasma. The time-dependent reflected signal is collected either by the transmitting antenna or by a nearby receiving antenna. The time-dependent product of the reflected signal and a local oscillator is accumulated.

The measurements are of two types: the coherent reflected signal strength measured at the transmitting antenna and the cross correlation between signals at a reference frequency ω_0 and a number of secondary frequencies ω_1, chosen so that the range of reflection points encompasses the turbulent correlation length. The cross-correlation signal monotonically decays with increasing separation between reflection points.

Various models have been applied to simulate the signal expected for models of turbulent fluctuations imposed on an otherwise smooth plasma profile. One-dimensional models, either in the geometrical optics approximation [6, 7] or in solutions of the full-wave equation [8–10], have been routinely used to infer the relation between measured correlation functions and the properties of the turbulent fluctuations. Bruskin *et al* [11, 12] analysed the resolution limit of

correlation reflectometry in two dimensions within the confines of the Born approximation. Mazzucato [13] computed scattering from two-dimensional turbulence in a planar plasma profile. Cohen *et al* [15] demonstrated the applicability of short-pulse reflectometry [16] to correlation reflectometry in two-dimensional simulations. Investigation of amplitude and phase variations arising during O-mode propagation in two-dimensional plasmas was studied by Irby *et al* [14] for several assumed forms of density fluctuation. Lin *et al* [17] solved the two-dimensional full-wave equation for a single scattering realization in realistic geometry, appropriate to Alcator CMOD. However, direct numerical solutions of the full-wave equations in two dimensions have had limited application to correlation analysis because of the substantial computational resources required to simulate a realistically sized system.

In this paper we describe a two-dimensional wave propagation code which has been constructed in order to help interpret the experimental signals from large-scale tokamak experiments. To facilitate quantitative comparison between computational and experimental results, the model includes a realistic antenna radiation pattern and the capability to input experimentally inferred two-dimensional profiles [18, 19] of density, electron temperature and magnetic field strength. We find that the convergence of the coherent and cross-correlation signals is quite slow with increasing ensemble size—typically several hundred realizations are required to obtain a meaningful result. An efficient computational algorithm is therefore a prerequisite if a model is to be a useful part of the data analysis process. The algorithm presented here is sufficiently fast (requiring 30 CPU seconds for computation of a single realization in a large tokamak) to make this practical. Efficiency is obtained by several means. First, the computational domain is divided into regions as shown in figure 1. The full-wave equation

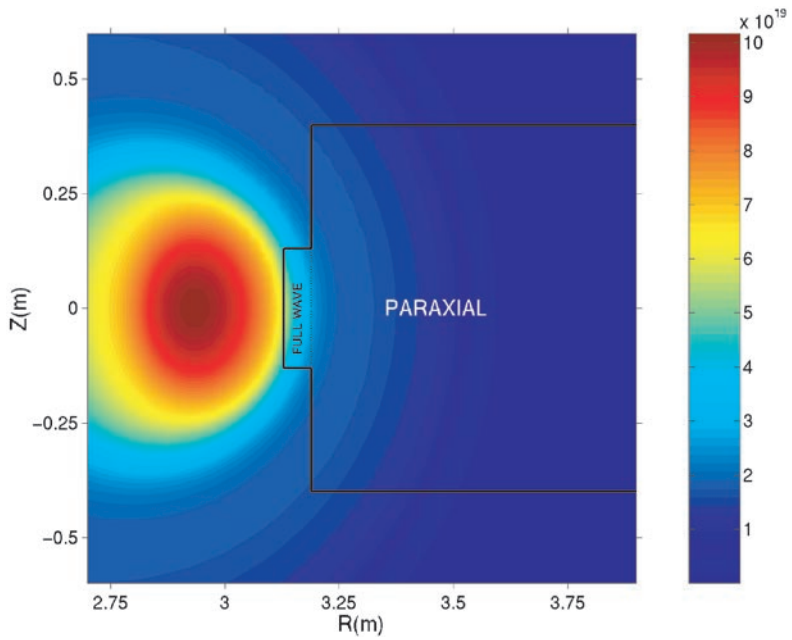

Figure 1. Electron density profile $N_e(R, Z)$ used for reflectometry simulations. The profile is reconstructed from TFTR Enhanced Reverse Shear shot #65601 at time 2.5 s. The rectangular domains labelled 'Full Wave' (respectively 'Paraxial Approximation') are the regions in which equation (1) (respectively equation (10)) are solved. The solutions are matched on the dotted strip $R = 319$ cm, -13 cm $\leqslant Z \leqslant 13$ cm.

is solved only where necessary (near the reflection layer). An implicit algorithm is used to speed approach to steady state. Elsewhere, computationally less demanding models suffice: the paraxial approximation is used in the underdense plasma. The wave field is projected through vacuum using the free-space Green's function.

The model is described in section 2. Results are presented in section 3, in which a comparison of one- and two-dimensional results for experimental profiles in a TFTR discharge is shown. It is found that the results of the two-dimensional correlation analysis bear a remarkable similarity to those obtained from the one-dimensional full-wave simulations over a wide range of turbulent scale lengths. Implications of this result for the interpretation of correlation reflectometry and future directions are presented in section 4.

2. Computational model

The propagation of the electric field amplitude $E(\boldsymbol{x}, t)$ is described by the wave equation

$$2\mathrm{i}\omega\frac{\partial E}{\partial t} + \mathcal{L}E = 0, \tag{1}$$

with

$$\mathcal{L} \equiv c^2\nabla^2 + \omega^2\epsilon, \tag{2}$$

where we have made the assumption of quasi-monochromaticity at frequency ω. Here $E(\boldsymbol{x}, t)$ is a complex field amplitude, in terms of which the full time–space variation is given as

$$\mathcal{E}(\boldsymbol{x}, t) = \mathrm{Re}[\exp(-\mathrm{i}\omega t)E(\boldsymbol{x}, t)], \tag{3}$$

where Re designates the real part. The time variation of $E(\boldsymbol{x}, t)$ is assumed slow compared to that of the phase factor. The plasma dielectric ϵ is modelled by the magnetized cold plasma X- or O-mode dielectric [20] with electron thermal corrections added [21, 22]. For large tokamaks, thermal effects result in significant shifts in the reflection point relative to the cold plasma result.

Since the wave transit time ($\sim L_n/v_{\mathrm{gr}} \sim 100\,\mathrm{cm}/c \sim 3\times10^{-9}$ s) is short compared to the time over which the turbulent fluctations vary ($\sim10^{-5}$ s), a set of steady solutions is computed for a given macroscopic profile and microwave parameters. The relative amplitude $\delta n_{\boldsymbol{k}s}$ of the microscopic fluctuations at each wavevector $\boldsymbol{k}$ for simulation s is assigned in terms of an assumed fluctuation spectrum $I_{\boldsymbol{k}}$, specifically $|\delta n_{\boldsymbol{k}s}| \propto I_{\boldsymbol{k}}^{1/2}$. The phases of the fluctuations are chosen randomly. Thus, for simulations s and s', and wavevectors $\boldsymbol{k}$ and $\boldsymbol{k}'$, the fluctuation correlation satisfies

$$\langle \delta n_{\boldsymbol{k}s}{}^{*}\delta n_{\boldsymbol{k}'s'}\rangle = \delta_{\boldsymbol{k}\boldsymbol{k}'}\delta_{ss'}\,I_{\boldsymbol{k}}. \tag{4}$$

The inverse Fourier transform of $\delta n_{\boldsymbol{k}}$ yields the relative fluctuation amplitude $\delta n(\boldsymbol{x})/n_0(\boldsymbol{x})$ where $n_0(\boldsymbol{x})$ is the smoothly varying equilibrium density profile. The total density

$$n(\boldsymbol{x}) = n_0(\boldsymbol{x})[1 + \delta n(\boldsymbol{x})]. \tag{5}$$

For comparison with experimental data, the spectral intensity is parameterized by an amplitude I_0, a mean wavevector $\boldsymbol{k}_{\mathrm{m}}$ and a two-dimensional width $\Delta\boldsymbol{k}$. The specific form chosen for the simulation results is

$$I_{\boldsymbol{k}} = I_0 \exp - \left\{ \left[\frac{(\boldsymbol{k}-\boldsymbol{k}_{\mathrm{m}})\cdot\hat{\boldsymbol{R}}}{\Delta\boldsymbol{k}\cdot\hat{\boldsymbol{R}}} \right]^2 + \left[\frac{(\boldsymbol{k}-\boldsymbol{k}_{\mathrm{m}})\cdot\hat{\boldsymbol{Z}}}{\Delta\boldsymbol{k}\cdot\hat{\boldsymbol{Z}}} \right]^2 \right\}, \tag{6}$$

where $\hat{\boldsymbol{R}}$ (respectively $\hat{\boldsymbol{Z}}$) are unit vectors in the radial (respectively vertical) directions in the poloidal plane. Many (usually several hundred) runs are made for a given choice (I_0, $\boldsymbol{k}_{\mathrm{m}}$, $\Delta\boldsymbol{k}$).

An average over the solution ensemble is identified with the experimentally obtained time series data.

A major challenge is that the computational domain—a poloidal cross section—measures many wavelengths in both dimensions. The wavelength of the probing radiation is set by the parameters at the desired reflecting layer. In large-scale tokamaks such as JT60 and TFTR, the wavelength is 2–3 mm. The distance between the antenna and reflecting layer is typically 2 m, of which approximately 50–100 cm is in plasma, with the remainder in vacuum. Propagation in vacuum is most efficiently handled by making use of the free-space Green's function to project the wave field between the antenna and plasma boundary. Considering, then, only the plasma region for direct numerical solution, the radial extent of the computational domain, $L_R \sim 400\lambda$. Even for a well-collimated incident beam, curvature of the reflecting layer and turbulent scattering typically lead to a finite cone angle of order $\pm 30^\circ$ for the reflected radiation. Thus the vertical extent L_Z is also of order 400λ.

An explicit solution of the wave equation requires a time step which satisfies the Courant stability condition. Assume discretization on a grid of cell size $\Delta d = \lambda/n_d$ with n_d points per wavelength in the $d = \{R, Z\}$ direction. Then, $\Delta t \leqslant \min(\Delta R, \Delta Z)/2c$, with c the speed of light. Solving for a time of order the crossing time $\tau_{\rm cr} \sim 2L_R/c$, requires $N_t = \max\{N_R, N_Z\}$ time steps with $N_d = n_d L_d/\lambda$. The CPU time per time step $\tau_{\rm step} = CN_R N_Z$, with $C \sim 5 \times 10^{-6}$ s on a fast RISC workstation. Typically $n_R = 20$, $n_Z = 2$, so that $N_t \sim 10^4$ and $N_R N_Z \sim 10^7$. A single such run takes of order 100 CPU hours. Hundreds of runs are required to achieve statistically significant results for a given set of parameters, making an explicit solution impractical.

For these reasons we use an implicit algorithm, which is stable for arbitrarily large time step, limited only by accuracy considerations. We write

$$\left(\frac{2\mathrm{i}\omega}{\Delta t} + \frac{1}{2}\mathcal{L}\right) E^{n+1} = S^n \tag{7}$$

for $E^{n+1} \equiv E[(n+1)\Delta t]$. Here the source

$$S^n = \left(\frac{2\mathrm{i}\omega}{\Delta t} + \frac{1}{2}\mathcal{L}\right) E^n$$

involves quantities at only the nth time level. Inversion of the Laplacian on the left-hand side then becomes the limiting step. By making use of the observation that, experimentally, the wavevectors are aligned principally along one of the (Cartesian) coordinate directions (R), an efficient iterative solution can be employed—the line Jacobi method [23]. Introducing iteration index m, the Laplacian ($\mathcal{L} = \mathcal{L}_R + \mathcal{L}_Z$) is solved directly in R and iteratively in Z:

$$\left(\frac{2\mathrm{i}\omega}{\Delta t} + \frac{1}{2}\mathcal{L}_R\right) E^{n+1,m} = -\frac{1}{2}\mathcal{L}_Z E^{n+1,m-1} + S^n\,. \tag{8}$$

Taking $m = 5$ is sufficient, given the rapid convergence.

The solution time for realistic large tokamak profiles on four Compaq 750 MHz Alpha 21264 processors (with domain decomposition into radial strips, and with essentially perfect scaling with processor number) is of order 10 min—marginally acceptable for required throughput.

Because $|c\nabla\epsilon/\omega\epsilon| \ll 1$ away from the reflection layer, further efficiency is obtained there through the use of the paraxial approximation. Defining the radial wavevector $k_R(R) \equiv \sqrt{\epsilon(R, Z_0)}$ and phase $\phi \equiv \int^R \mathrm{d}R\, k_R$ along the centroid, $Z = Z_0$, of the incident wave packet and decomposing the field into incoming (I) and reflected (R) components,

$$E(\boldsymbol{x}, t) = E_{\rm PI} \exp(-\mathrm{i}\phi) + E_{\rm PR} \exp(\mathrm{i}\phi), \tag{9}$$

we have, away from the reflection point,

$$\pm 2\mathrm{i}\frac{\partial}{\partial R}k_R^{1/2}E_\mathrm{P} + \mathcal{L}_Z k_R^{1/2}E_\mathrm{P} + [\epsilon(R, Z) - \epsilon(R, Z_0)]k_R^{1/2}E_\mathrm{P} = 0, \tag{10}$$

with the + (respectively −) sign taken for E_PI (respectively E_PR) and where the time variation is ignored as slow compared to the wave transit time across the simulation domain. Again, the solution in R is done implicitly, requiring an inversion of $\mathcal{L}_Z$. This is done directly through Gaussian elimination.

In summary, as shown in figure 2, the computation proceeds as follows:

(a) Specify the (complex) incident amplitude at the antenna plane.
(b) Project the incident amplitude onto the plasma boundary using the free-space Green's function.
(c) Solve the paraxial equation for E_PI up to a surface $R = R_\mathrm{FW}$ within a few wavelengths of the reflection point.
(d) From R_FW inward solve the full-wave equation, equation (1), implicitly for E, with E_PI as the incoming wave amplitude. Advance the solution until steady state is reached.

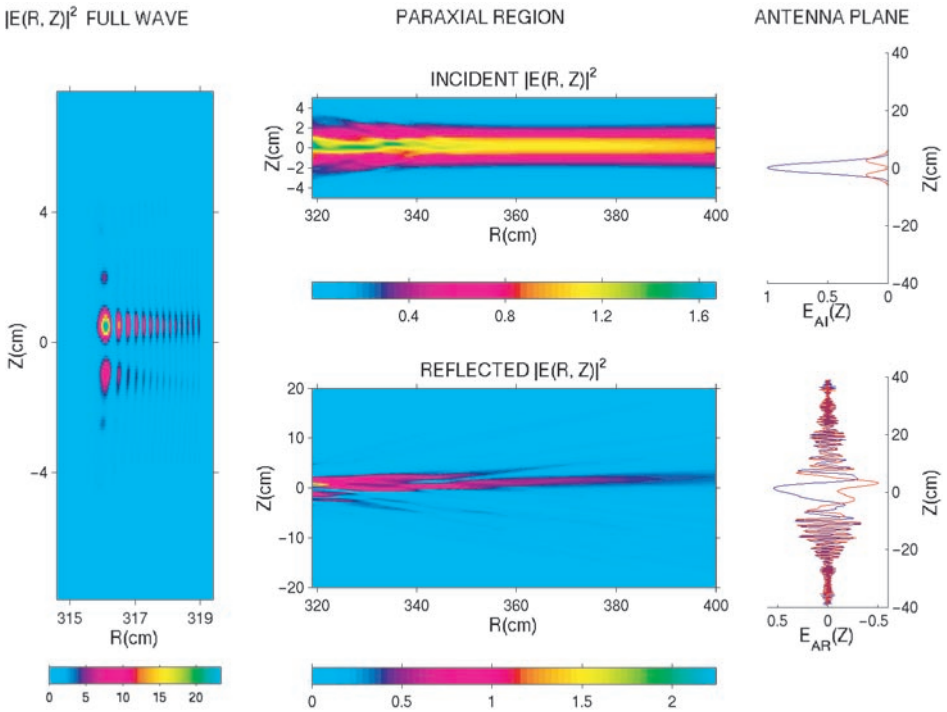

Figure 2. Counterclockwise, from upper right: (a) Real (blue) and imaginary (red) components of the prescribed incident field amplitude $E_\mathrm{AI}(Z)$ at the antenna plane, $R = 400$ cm. Pseudocolour plots of: (b) The intensity of the incident component $|E_\mathrm{PI}(R, Z)|^2$ in the paraxial domain and (c) $|E(R, Z)|^2$ in the full-wave region. (d) The intensity of the reflected component $|E_\mathrm{PR}(R, Z)|^2$ in the paraxial domain. (e) The final subplot shows the outgoing field amplitude $E_\mathrm{AR}(Z)$ at the antenna plane, as in subplot (a). The pseudocolour plots extend over subsets of the respective computational domains in which the field strengths are non-negligible. The computational domain for the paraxial solution extends from 319 cm $\leqslant R \leqslant$ 400 cm, −40 cm $\leqslant Z \leqslant$ 40 cm. The computational domain for the full-wave solution extends from 313 cm $\leqslant R \leqslant$ 319 cm, −13 cm $\leqslant Z \leqslant$ 13 cm.

(e) Take the outgoing component E_{R} of E as an initial condition for the reflected paraxial field

$$E_{\mathrm{PR}}(R_{\mathrm{FW}}, Z) = E_{\mathrm{R}}(R_{\mathrm{FW}}, Z). \tag{11}$$

Apply step (c), then step (b) in the outgoing direction to compute the amplitude of the reflected field at the receiver plane.

The method is efficient and accurate. A single realization for a system size of $360 \times 240\lambda^2$ takes 30 CPU seconds to solve on a single alpha processor.

3. Results

A principal result of the computations is the value of both the coherent reflected signal, $g(\omega)$, and the cross correlation $r(\omega_0, \omega_1)$. These are constructed from the numerical results as follows: for probe frequency ω, let $E_{\mathrm{AI}}(\omega, Z)$ and $E_{\mathrm{AR}}(\omega, Z)$ designate the complex incident and reflected field amplitudes at $R = R_{\mathrm{A}}$, with R_{A} the radius of the antenna plane (figure 2, right-hand side). For any function $\Phi(R = R_{\mathrm{A}}, Z)$, define the projection

$$M(\omega) \equiv \int \mathrm{d}Z\, E_{\mathrm{AR}}(\omega, Z) E^*_{\mathrm{AI}}(\omega, Z). \tag{12}$$

Let $\langle\,\rangle$ denote an average over the run ensemble. Then

$$g(\omega) \equiv \frac{\langle M(\omega)\rangle}{\sqrt{\langle |M(\omega)|^2\rangle}} \tag{13}$$

and

$$r(\omega_0, \omega_1) \equiv \frac{\langle M(\omega_0) M(\omega_1)\rangle}{\sqrt{\langle |M(\omega_0)|^2\rangle \langle |M(\omega_1)|^2\rangle}}. \tag{14}$$

Results for g and r from two series of two-dimensional simulations are presented in figure 3 (symbols), together with their values as calculated from a one-dimensional full-wave simulation (solid lines). Both were done for a typical TFTR plasma (shot #65601, at time 2.5 s). The main plasma parameters are: major radius 2.93 m, minor radius 1.06 m, magnetic field 4.0 T, central density $1.0 \times 10^{20}\,\mathrm{m}^{-3}$ and central electron temperature 7.0 keV. X-mode waves were launched horizontally into the plasma midplane at 11 frequencies between 121 and 137 GHz (vacuum wavelengths between 0.248 and 0.219 cm) from an antenna of focal length 135 cm located at $R = 400$ cm, $Z = 0$.

One series (left-hand side of figure 3) was performed for a turbulent radial correlation length $\lambda_{cR} = 0.2$ cm, the other for $\lambda_{cR} = 2.0$ cm. The poloidal correlation length $\lambda_{cZ} = 0.4$ cm. The short poloidal correlation length was chosen so as to maximize the difference expected between two- and one-dimensional simulations. The volume-averaged relative fluctuation level $f = \int_V \mathrm{d}^2x\, (\delta n/n)^2 / V = 2.5 \times 10^{-5}$. These parameters were achieved by choosing, in equation (6), $\Delta\boldsymbol{k} \cdot \hat{\boldsymbol{R}} = 10$ and $1\,\mathrm{cm}^{-1}$, $\Delta\boldsymbol{k} \cdot \hat{\boldsymbol{Z}} = 5\,\mathrm{cm}^{-1}$, $\boldsymbol{k}_{\mathrm{m}} = 0$ and $I_0 = 4\pi(\Delta\boldsymbol{k} \cdot \hat{\boldsymbol{R}})(\Delta\boldsymbol{k} \cdot \hat{\boldsymbol{Z}}) f$.

It can be seen that the calculated two-dimensional cross correlation agrees remarkably well with the one-dimensional calculations [10] over this wide variation of radial correlation lengths. The fact that the coherent reflected signal is systematically higher in the two-dimensional calculations can be explained by the scattering of waves out of the receiver aperture. Nevertheless, it is remarkable that the one- and two-dimensional coherent reflection coefficients bear such a strong similarity, given the very short poloidal correlation lengths used in these simulations. For comparison with $|r|$, the respective turbulent radial correlation functions are plotted as dashed lines in the upper figures, from which the radial resolution

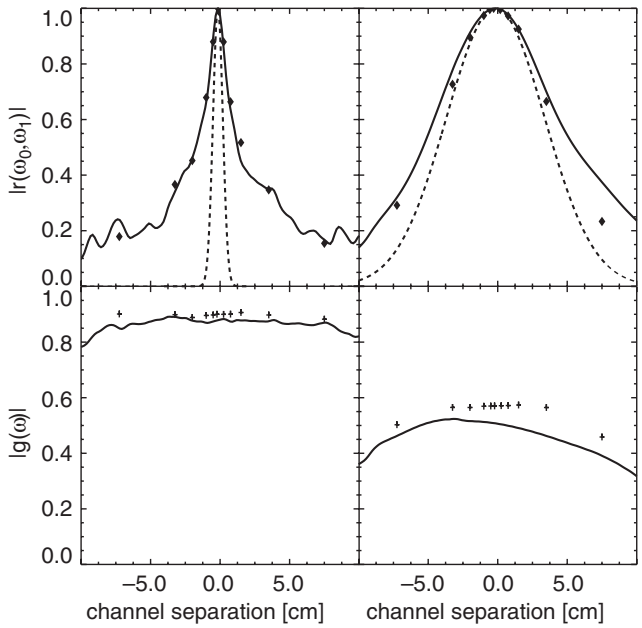

Figure 3. Top: magnitude of the cross-correlation coefficient $|r(\omega_0, \omega_1)|$ versus the separation between reflection points from one-dimensional (——) and two-dimensional (♦) simulations. Bottom: the magnitude of coherent signal $|g(\omega)|$ versus location of the reflection point at the plasma midplane relative to that for $f = 128$ GHz. Solid lines (respectively crosses) are results of one-dimensional (respectively two-dimensional) simulations. Left-hand plots are for a radial correlation length $\lambda_{cR} = 0.2$ cm. Right-hand plots are for $\lambda_{cR} = 2.0$ cm. The dashed lines in the upper figures show the turbulent radial correlation function which generated the fluctuation ensemble in each case. Other parameters: volume averaged relative fluctuation level $= 2.5 \times 10^{-5}$, poloidal correlation length $\lambda_{cZ} = 0.4$ cm.

limit appears to be about 1 cm. This is somewhat larger than would be obtained from previous estimates, which range from the free-space wavelength of the probing radiation [8] ($\lambda_0 = 0.23$ cm) to the width of the last Airy fringe near the turning point [1]

$$W_{\text{Airy}} = 0.48 L_n^{1/3} \lambda_0^{2/3}, \tag{15}$$

expressed here in terms of λ_0 and the local density gradient scale length $L_n = |n/\nabla n|$. Taking a radial cut of the density profile at the vertical midplane yields an estimate $L_n = 10.2$ cm at the turning point (approximately 316 cm), which yields $W_{\text{Airy}} = 0.39$ cm.

Figure 4 shows the variation in $|g|$ with number of runs in the ensemble. Because of the slow rate of convergence, 500 simulations were performed at each frequency. Thus, each point in figure 3 represents an ensemble average of 500 separate runs.

A measure of the resolution expected from correlation reflectometry is shown in figure 5 where the full-width half maximum of $|r|$ is plotted versus that of the radial density correlation length both from the two-dimensional simulations (squares) as well as from a series of one-dimensional simulations (solid line). Again, one- and two-dimensional results are nearly identical and indicate a resolution limit <1 cm. For comparison, the value of W_{Airy} is shown as a vertical line.

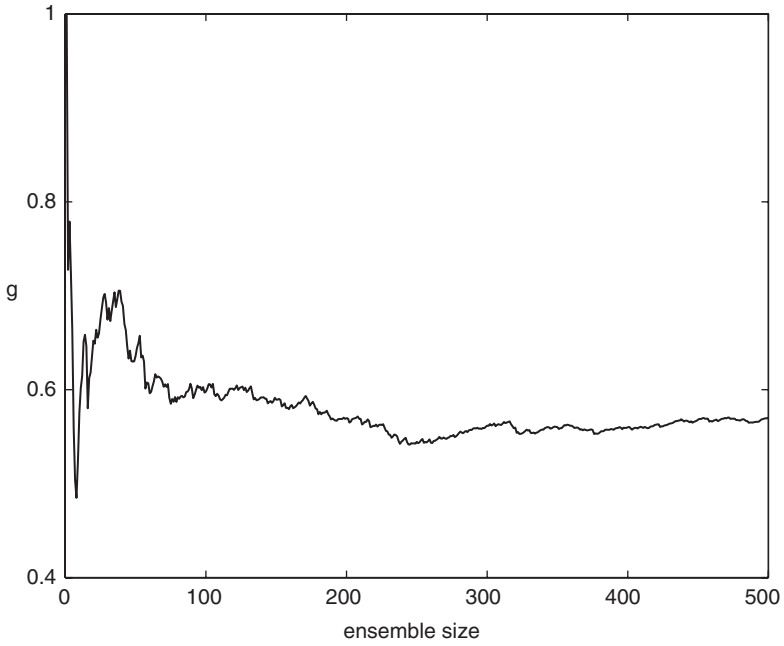

Figure 4. Measurement of the ensemble averaged coherent reflected signal g, equation (13), at a probe frequency of 128 GHz versus the number of simulations included in the ensemble.

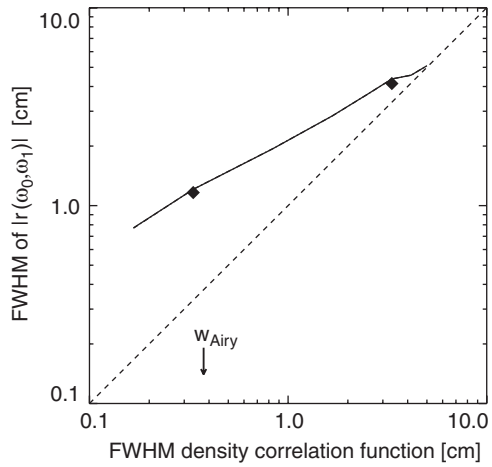

Figure 5. Measured value of the full-width half maximum of $|r(\omega_0, \omega_1)|$ versus that of the density correlation function from full-wave one-dimensional simulations (——) and two-dimensional simulations (■). The value of the width of the last Airy fringe, W_{Airy}, as given by equation (15), is shown as a vertical line.

4. Discussion

The surprising result of this analysis is that the correlation and coherent reflection level is essentially identical to that obtained with a one-dimensional full-wave analysis despite the fact that the transverse wavenumber of the perturbations is of the order of the wavelength of the

probing beam. To understand this result in greater detail, many more simulations are certainly required. However, in a recent work [17], it was pointed out that the curvature of the reflecting layer can have a significant effect to broaden the spectral response of the receiver for high transverse wavenumbers. Similar results have also been obtained using a two-dimensional full-wave analysis on the JT-60U tokamak [24], suggesting that the close correspondence of two- and one-dimensional simulations observed in our analysis may also hold for other large-scale devices. However, the same analysis outlined in this paper needs to be repeated on a case-by-case basis to confirm the similarity of two- and one-dimensional simulations. Indications that the two- and one-dimensional simulations can also diverge significantly in their predictions is shown in the case of X- to O-mode correlation reflectometry performed on a laboratory-scale facility [10]. In that case, the different radiation patterns at the reflecting layer for very different wave frequencies can lead to a degradation of the correlation coefficient at low fluctuation levels which is not apparent in the one-dimensional analysis.

These results were computed only for microwave beams launched normal to the surface of reflection. An important issue for future investigation is how sensitive the correspondence of the one- and two-dimensional simulations of the radial correlation are to small angles of misalignment of the waves incident on the reflecting layer or for a receiver slightly misaligned to the direction of specular reflection. Such systematic studies of correlation reflectometry in large-scale facilities are now computationally tractable with the advent of efficient full-wave algorithm as discussed in this study.

5. Conclusion

A two-dimensional simulation program has been developed specifically to model reflectometry measurements in large tokamaks. By implementing algorithms tailored to the vacuum, underdense plasma and reflection layer regions, the high efficiency required for statistical studies has been achieved.

Results have been presented for a relatively large and relatively short radial correlation length of model density fluctuations. These results pertain to waves injected at normal incidence to the surface of reflection. Future studies will include an investigation of the degree to which the correspondence of one- and two-dimensional simulations breaks down with oblique angles of incidence.

The authors thank Doug McCune for help with the importation of TRANSP generated TFTR profiles. This work was funded by DOE Contract No DE-AC02-76CH03073.

References

[1] Nazikian R, Kramer G J and Valeo E 2001 *Phys. Plasma* **8** 1840
[2] Mazzucato E and Nazikian R 1991 *Plasma Phys. Control. Fusion* **33** L261
[3] Gilmore M, Peebles W A and Nguyen X V 2000 *Plasma Phys. Control. Fusion* **42** 655
[4] Gilmore M, Peebles W A and Nguyen X V 2000 *Rev. Sci. Instrum.* **72** 293
[5] Nazikian R *et al* 1998 IAEA-CN-69/PDP/03, paper presented at *17th IAEA Conf. on Fusion Energy (Yokohama)*
[6] Nazikian R and Mazzucato E 1995 *Rev. Sci. Instrum.* **66** 392
[7] Cohen B I, Hooper E B, Spang M C and Dornier C W 1999 *Rev. Sci. Instrum.* **70** 1407
[8] Bretz N 1992 *Phys. Fluids* B **4** 2414
[9] Hutchinson I H 1992 *Plasma Phys. Control. Fusion* **34** 1225
[10] Kramer G J, Nazikian R and Valeo E 2002 *Plasma Phys. Control. Fusion* **44** L11
[11] Bruskin L G, Mase A and Tamano T 1995 *Plasma Phys. Control. Fusion* **37** 255
[12] Bruskin L G, Mase A and Tamano T 1997 *Fusion Eng. Design* **34–35** 441
[13] Mazzucato E 1998 *Rev. Sci. Instrum.* **69** 1691

[14] Irby J H, Horne S, Hutchinson I H and Stek P C 1993 *Plasma Phys. Control. Fusion* **35** 601
[15] Cohen B I, Kaiser T B and Garrison J C 1997 *Rev. Sci. Instrum.* **68** 1238
[16] Cohen B I, Hooper E B, Kaiser T B, Williams E A and Dornier C W 1999 *Phys. Plasma* **6** 1732
[17] Lin Y, Nazikian R, Irby J H and Marmar E S 2001 *Plasma Phys. Control. Fusion* **43**
[18] Hawryluk R J 1980 An empirical approach to tokamak transport *Physics of Plasmas Close to Thermonuclear Conditions* vol 1, ed B Coppi *et al* (Brussels: CEC) p 19
[19] Ongena J, Evrard M and McCune D 1998 *Proc. 3rd Carolus Magnus Summer School on Plasma Physics (Belgium: Spa)* as published in *Transactions of Fusion Technology* **33** (2T) 181
[20] Stix T H 1992 *Waves in Plasmas* (New York: American Institute of Physics) section 2-7
[21] Mazzucato E 1992 *Phys. Fluids* B **4** 3460
[22] Bindslev H 1993 *Plasma Phys. Control. Fusion* **35** 1093
[23] Vu H X 1998 *J. Comput. Phys.* **144** 257
[24] Nazikian R, in preparation